

S. Liebig* · U.-G. Meißner** · A. Nogga***

Jacobi no-core shell model for p -shell nuclei

Received: July 3, 2021/ Accepted: date

Abstract We introduce an algorithm to obtain coefficients of fractional parentage for light p -shell nuclei. The coefficients enable to use Jacobi coordinates in no-core shell model calculations separating off the center-of-mass motion. Fully antisymmetrized basis states are given together with recoupling coefficients that allow one to apply two- and three-nucleon operators. As an example, we study the dependence on the harmonic oscillator frequency of ${}^3\text{H}$, ${}^4\text{He}$, ${}^6\text{He}$, ${}^6\text{Li}$ and ${}^7\text{Li}$ and extract their binding and excitation energies. The coefficients will be made openly accessible as HDF5 data files.

Keywords no-core shell model · p -shell nuclei · binding energies · coefficients of fractional parentage

1 Introduction

One of the major goals of nuclear physics is to understand properties of nuclei based on nuclear two-, three- and maybe more-body interactions. To this aim, methods have to be devised that allow one to predict such properties based on these interactions. In the very light systems, calculations are often directly done in configuration or momentum space [1; 2; 3; 4]. Calculations using special basis sets, e.g. hyperspherical harmonics [5; 6], Sturmians [7] or harmonic oscillator (HO) states [8], are also able to provide accurate solutions for the light systems but become the tool of choice for systems larger than $A = 4$.

Here we will concentrate on the no-core shell model (NCSM) that has become a standard method to perform nuclear structure calculations for p -shell nuclei (for recent applications see e.g. [8; 9; 10]) and is based on an expansion in terms of HO states. Although the Gaussian long distance behavior of the HO states is not particularly well suited for the description of the long distance behavior of nuclear wave functions [11], the basis enables one to separate out the center-of-mass (CM) motion exactly and, which will be important below, to perform exact transformation between different choices of coordinates within a finite set of HO states. Binding energies and especially excitation energies do not

* s.liebig@fz-juelich.de

** meissner@hiskp.uni-bonn.de

*** a.nogga@fz-juelich.de

S. Liebig · U.-G. Meißner · A. Nogga
Institute for Advanced Simulation, Institut für Kernphysik, and Jülich Center for Hadron Physics,
Forschungszentrum Jülich, D-52425 Jülich, Germany

S. Liebig · U.-G. Meißner · A. Nogga
JARA – High Performance Computing, Forschungszentrum Jülich, D-52425 Jülich, Germany

U.-G. Meißner
Helmholtz-Institut für Strahlen- und Kernphysik and Bethe Center for Theoretical Physics, Universität Bonn,
D-53115 Bonn, Germany

depend strongly on the long range behavior of the wave function and can therefore be predicted with high accuracy except for states that are dominated by HO excitations as for example α -cluster states. Other schemes, like nuclear lattice calculations, are more suited for such states [12]. Nevertheless, due to its flexibility with respect to interactions, the NCSM became particularly useful for the study of chiral nucleon-nucleon (NN) and three-nucleon (3N) interactions [13; 14; 15]. Using an importance truncation scheme, the extension to more complex nuclei is possible [9].

Whereas s -shell nuclei are usually calculated using Jacobi coordinates within the NCSM [16], more complex systems have so far been mostly calculated using the so-called m -scheme basis where all nucleons are described by single particle states. This avoids the difficult antisymmetrization of states expressed in Jacobi coordinates. The price for this simplification is that the CM motion cannot be explicitly separated out anymore leading to much larger dimensions of the linear equations to be solved and. Furthermore, expensive transformations of interaction matrix elements from relative coordinates to single particle coordinates are necessary. Often these transformations have to be performed on-the-flight since matrix elements of the interactions cannot be stored in the single particle basis due to memory constraints. These constraints are especially relevant since it is clear by now that, for accurate calculations, chiral nuclear interactions of high order in chiral expansion are required [17; 18] which implies that even four-nucleon interactions might be relevant [19; 20; 21]. The on-the-flight transformation of such interactions will be tremendously more difficult.

The NCSM describes many-body systems containing A point-like non-relativistic nucleons in the HO basis where all A nucleons of the system are considered to be active [8]. This HO basis allows one to represent the full complexity of nuclear interactions efficiently. But in order to reach converged results in practical calculations, the interactions have to be soft and should not include the strong repulsion which is part of most nuclear interaction models. In order to be able to study nuclear systems, most of the standard interactions are only the starting point for obtaining a soft effective interaction. Early NCSM calculations relied on a decoupling formulated specifically for HO spaces (see e.g. [13] for a summary of this approach). In this case, the effective interactions depend on the HO frequency and model space size and are useful only for NCSM calculations. As within all approaches to effective interactions, many-body forces are induced. These have been included up to the level of three-nucleon forces (3NFs) [22] which is sufficient to obtain converged results. But this approach has several disadvantages. The most important one is probably, that the effective interaction cannot be used elsewhere, e.g. in Faddeev-Yakubovsky or even coupled-cluster calculations so that it is difficult to benchmark results and to check that induced many-body forces do not have large effects on other observables. The convergence pattern for these interactions is also more complicated since convergence for binding energies can be reached from above and below. These disadvantages can be circumvented using interactions that either constrain the interactions to low momenta as in the case of V_{lowk} [23] or decouple low- and high momentum components using the similarity renormalization group (SRG) [24]. In both cases, the interactions become soft enough so that converged results can be obtained. In recent years, SRG has become the tool of choice since it is also possible to obtain induced 3NFs [25]. Our test calculations below are therefore also based on this approach.

The subject of this work is to come back to the development of a Jacobi relative coordinate NCSM started in [16] and extend it towards p -shell nuclei. The main difficulty is to build up an antisymmetrized set of nuclear HO states using Jacobi relative coordinates. Our algorithm to obtain these states is described in Section 2. These states alone are still not useful for applications. In order to be able to calculate matrix elements of two-body operators, we also need recoupling coefficients that separate out NN states from the A -body system. In Section 3, it is summarized how these transitions can be done. This is then extended to transition coefficients that separate out 3N clusters in Section 4. Such coefficients will be important in future to apply 3N interactions within this scheme. Using the new antisymmetrized states and the transitions to states that single out an NN subsystem allows us to do first example calculations for the binding and excitation energies for light nuclei in Section 5. We use a new, mostly automatized scheme to extract binding energies and estimates of the numerical error from our results, which can be particularly easy performed based on the Jacobi basis states since binding energy calculations can be done for a wide range of HO frequencies. Once the antisymmetrized basis states are obtained, the individual binding energy calculations are not computationally expensive anymore since the states are independent of the interaction and the HO frequency. In the appendices, we summarize the implications of the conventions used for HO wave functions and list the sets of antisymmetrized HO states and transition coefficients that have been generated.



Fig. 1 Three-cluster Jacobi coordinates. The left hand side singles out the third particle as spectator. The right hand side singles out the second one. The arrow defines the direction of corresponding relative momenta or positions. This direction defines the phases depending on the corresponding angular momenta.

2 Antisymmetrized HO states in a Jacobi basis

The Schrödinger equation for the internal motion of the A -nucleon system reads

$$\begin{aligned}
 H_A &= \sum_{i=1}^A \frac{k_i^2}{2m} + \sum_{i<j=1}^A V_{ij} + \sum_{i<j<k=1}^A V_{ijk} - \frac{\mathbf{P}^2}{2M} \\
 &= \sum_{i<j=1}^A \frac{2}{A} \frac{\mathbf{p}_{ij}^2}{m} + \sum_{i<j=1}^A V_{ij} + \sum_{i<j<k=1}^A V_{ijk}.
 \end{aligned} \tag{1}$$

Here the CM kinetic energy $\frac{\mathbf{P}^2}{2M}$, where M is the total mass of the A -nucleon system and \mathbf{P} the CM momentum, is subtracted to obtain the internal energy. We included 2N interactions of the pair (ij) (V_{ij}) and 3N interactions of the triplet (ijk) (V_{ijk}). The expression is rewritten such that the individual momenta \mathbf{k}_i of the nucleons are replaced by pair momenta $\mathbf{p}_{ij} = \frac{1}{2}(\mathbf{k}_i - \mathbf{k}_j)$. m is the mass of the nucleon. Here, we neglect the small difference of proton and neutron mass.

We will solve this equation in a basis $|\alpha\rangle$ of antisymmetrized HO states

$$\langle \alpha | H_A | \beta \rangle \langle \beta | \Psi \rangle = E \langle \alpha | \Psi \rangle \tag{2}$$

where a sum over all these HO states $|\beta\rangle$ is implied. The difficulty is to define the set of antisymmetrized states in Jacobi coordinates.

2.1 General set of Jacobi coordinates for three clusters

In order to find these antisymmetrized states, we start from a general set of Jacobi coordinates for a system of three clusters 1, 2 and 3. Each of the clusters is characterized by its mass, total angular momentum and total isospin, $m_{1,2,3}$, $s_{1,2,3}$ and $t_{1,2,3}$. The motion is then described by the motion within the pair (i.e. (12)) and the motion of the spectator 3. For an HO basis, the corresponding basis reads

$$| n_{12} n_3 ((l_{12} (s_1 s_2) S_{12}) J_{12} (l_3 s_3) I_3) J; ((t_1 t_2) T_{12} t_3) T \rangle \tag{3}$$

where n_{12} (n_3) is the HO quantum number for the relative motion of 1 and 2 (of the spectator 3), l_{12} (l_3) the corresponding orbital angular momenta, S_{12} , J_{12} and I_3 are the pair spin, pair total angular momentum and the total angular momentum of the spectator and J is the total angular momentum of the system. The isospins of the pair couple to T_{12} which combines with the isospin of the spectator particle to the total isospin T . The states are eigenstates of HO in the relative coordinates

$$H_{HO,rel} = \frac{\mathbf{p}_{12}^2}{2\mu_{12}} + \frac{\mathbf{p}_3^2}{2\mu_3} + \frac{1}{2}\mu_{12}\omega^2 \mathbf{r}_{12}^2 + \frac{1}{2}\mu_3\omega^2 \mathbf{R}_3^2. \tag{4}$$

where the reduced masses are defined as

$$\mu_{12} = \frac{m_1 m_2}{m_1 + m_2}, \quad \mu_3 = \frac{(m_1 + m_2) m_3}{m_1 + m_2 + m_3} \tag{5}$$

and the relative coordinates in terms of single cluster coordinates (momenta) \mathbf{r}_i (\mathbf{k}_i) are given by

$$\begin{aligned} \mathbf{r}_{12} &= \mathbf{r}_1 - \mathbf{r}_2, & \mathbf{p}_{12} &= \frac{m_2}{m_1 + m_2} \mathbf{k}_1 - \frac{m_1}{m_1 + m_2} \mathbf{k}_2 \\ \mathbf{R}_3 &= \mathbf{r}_3 - \frac{m_1 \mathbf{r}_1 + m_2 \mathbf{r}_2}{m_1 + m_2}, & \mathbf{p}_3 &= \frac{m_1 + m_2}{m_1 + m_2 + m_3} \mathbf{k}_3 - \frac{m_3}{m_1 + m_2 + m_3} (\mathbf{k}_1 + \mathbf{k}_2). \end{aligned} \quad (6)$$

Here we omitted the internal state of the clusters since it will only become relevant later. This kind of Jacobi coordinate is depicted on the left hand side of Fig. 1. Note that the direction of the arrows defines the direction of corresponding relative positions or momenta as given above.

For such a general set of Jacobi coordinates, we need to perform a coordinate transformation to the Jacobi coordinates depicted on the right hand side of Fig. 1. Such a transformation does not change the internal motion of the clusters and the total parity, angular momentum and isospin. For an HO basis, the corresponding states read

$$| n_{13} n_2 ((l_{13} (s_1 s_3) S_{13}) J_{13} (l_2 s_2) I_2) J ((t_1 t_3) T_{13} t_2) T \rangle \quad (7)$$

and singles out the second particle as the spectator with corresponding definitions of the relative coordinates and momenta. A special property of HO states is that also the total HO energy quantum number

$$\mathcal{N} = 2n_{12} + l_{12} + 2n_3 + l_3 = 2n_{13} + l_{13} + 2n_2 + l_2 \quad (8)$$

is conserved.

In order to relate the spatial part of the transitions to Talmi-Moshinsky brackets [26; 27], we introduce dimensionless relative coordinates using the oscillator lengths $b_{12} = \sqrt{\frac{1}{\mu_{12} \omega}}$ and $b_3 = \sqrt{\frac{1}{\mu_3 \omega}}$

$$\boldsymbol{\rho}_{12} = \frac{\mathbf{r}_{12}}{b_{12}}, \quad \boldsymbol{\rho}_3 = \frac{\mathbf{R}_3}{b_3}. \quad (9)$$

The coordinate transformation can then be put into the form of Ref. [28]

$$\begin{pmatrix} \boldsymbol{\rho}_{13} \\ -\boldsymbol{\rho}_2 \end{pmatrix} = \begin{pmatrix} \sqrt{\frac{d}{1+d}} & \sqrt{\frac{1}{1+d}} \\ \sqrt{\frac{1}{1+d}} & -\sqrt{\frac{d}{1+d}} \end{pmatrix} \begin{pmatrix} \boldsymbol{\rho}_{12} \\ -\boldsymbol{\rho}_3 \end{pmatrix} \quad (10)$$

where $d = \frac{m_2 m_3}{m_1 (m_1 + m_2 + m_3)}$. Note that the additional minus signs required in front of $\boldsymbol{\rho}_2$ and $\boldsymbol{\rho}_3$ need to be taken into account by an extra phase factor $(-)^{l_2+l_3}$. The spatial part is therefore given by the corresponding HO bracket. The spin and isospin part just requires recoupling. One therefore finds for the general coordinate transformation

$$\begin{aligned} & \langle n_{13} n_2 ((l_{13} (s_1 s_3) S_{13}) J_{13} (l_2 s_2) I_2) J ((t_1 t_3) T_{13} t_2) T | n_{12} n_3 ((l_{12} (s_1 s_2) S_{12}) J_{12} (l_3 s_3) I_3) J ((t_1 t_2) T_{12} t_3) T \rangle \\ &= \hat{J}_{13} \hat{I}_2 \hat{J}_{12} \hat{I}_3 \sum_{LS} \hat{L}^2 \hat{S}^2 \begin{Bmatrix} l_{13} & S_{13} & J_{13} \\ l_2 & s_2 & I_2 \\ L & S & J \end{Bmatrix} \begin{Bmatrix} l_{12} & S_{12} & J_{12} \\ l_3 & s_3 & I_3 \\ L & S & J \end{Bmatrix} \\ & (-1)^{l_2+l_3} \langle n_{13} l_{13}, n_2 l_2 : L | n_{12} l_{12}, n_3 l_3 : L \rangle_d \\ & (-1)^{S_{13}+s_2+S_{12}+s_3} \hat{S}_{13} \hat{S}_{12} \begin{Bmatrix} s_2 & s_1 & S_{12} \\ s_3 & S & S_{13} \end{Bmatrix} (-1)^{T_{13}+t_2+T_{12}+t_3} \hat{T}_{13} \hat{T}_{12} \begin{Bmatrix} t_2 & t_1 & T_{12} \\ t_3 & T & T_{13} \end{Bmatrix}. \end{aligned} \quad (11)$$

For quantum numbers, we use the abbreviation $\hat{l} = \sqrt{2l+1}$. The HO bracket $\langle n_{13} l_{13}, n_2 l_2 : L | n_{12} l_{12}, n_3 l_3 : L \rangle_d$ follows the conventions of [28] and the mass ratio d is given above. In Appendix A, we summarize explicitly which configuration and momentum space HO wave functions are implied by these conventions.

Table 1 Labeling and graphical representation of different sets of coordinates for the A -body system.

label	graphical rep.	subsystems	dimensionality
$\alpha^{*(1)}$		$\alpha_{A-1} + N$	$A \times \text{grey circle}$
$(\alpha^{*(1)})^{*(1)}$		$\alpha_{A-1}^{*(1)} + N$	$(A-1) \times \text{grey circle} \times \text{black dot}$ $= (A-1) \times A \times \text{grey circle}$
$\alpha^{*(2)}$		$\alpha_{A-2} + \alpha_{12}$	$\frac{1}{2} \times \text{grey circle} \times \text{black dot}$ $= \frac{(A-1)}{2} \times \text{grey circle} \times \text{black dot}$ $= \frac{A(A-1)}{2} \times \text{grey circle}$
$(\alpha^{*(1)})^{*(2)}$		$\alpha_{A-2}^{*(1)} + \alpha_{12}$	$(A-2) \times \text{grey circle} \times \text{black dot}$ $= \frac{A(A-1)(A-2)}{2} \times \text{grey circle}$
$(\alpha^{*(1)})^{*(A-3)}$		$\alpha_3^{*(1)} + \alpha_{A-3}$	$\approx \text{grey circle} \times \text{black dot}$ $= (A-2) \times \text{grey circle} \times \text{black dot}$ $= \frac{A(A-1)(A-2)}{2} \times \text{grey circle}$
$\alpha^{*(3)}$		$\alpha_{A-3} + \alpha_3$	$\frac{1}{3} \times \text{grey circle} \times \text{black dot}$ $= \frac{(A-2)}{3} \times \text{grey circle} \times \text{black dot}$ $= \frac{A(A-1)(A-2)}{6} \times \text{grey circle}$

For the case that clusters/particles 2 and 3 are identical, the coordinate transformations are equivalent to transposition operators

$$\begin{aligned}
& {}_{(13)2} \langle n_{13} n_2 ((l_{13} (s_1 s_3) S_{13}) J_{13} (l_2 s_2) I_2) J ((t_1 t_3) T_{13} t_2) T | \\
& \quad | n_{12} n_3 ((l_{12} (s_1 s_2) S_{12}) J_{12} (l_3 s_3) I_3) J ((t_1 t_2) T_{12} t_3) T \rangle_{(12)3} \\
& \equiv {}_{(12)3} \langle n_{13} n_2 ((l_{13} (s_1 s_2) S_{13}) J_{13} (l_2 s_3) I_2) J ((t_1 t_2) T_{13} t_3) T | \\
& \quad \mathcal{P}_{23} | n_{12} n_3 ((l_{12} (s_1 s_2) S_{12}) J_{12} (l_3 s_3) I_3) J ((t_1 t_2) T_{12} t_3) T \rangle_{(12)3} . \tag{12}
\end{aligned}$$

We added subscripts $(ij)k$ to the states to make the clusters involved in the subsystem and the spectator explicit. Note that, for the right hand side, this implies that the quantum number S_{13} and T_{13} are total spins and isospins related to s_1, s_3, t_1 and t_3 . Correspondingly, the labels of the other quantum numbers are related to the (12) subsystem and spectator 3 even if the labels of the quantum numbers are different. Below, we will explicitly show how quantum numbers of the A -nucleon system are related to the the quantum numbers in Eq. (11).

2.2 Antisymmetrization of A -body states

These relations are the basis of all following expressions. The calculations often require to represent basis states in terms of states of subclusters. In Table 1, we have summarized the labeling of such states. In short, states are labeled by a greek letter that indexes all possible states for a set of given quantum numbers. A superscript $*(i)$ indicates that an i -particle subcluster has been separated off from the



Fig. 2 Two representations of $|(\alpha^{*(1)})^{*(1)}\rangle$ coordinates used for the antisymmetrization operator. The arrangement matches the general coordinates shown in Fig. 1. Note that the direction of the coordinates differs for the subsystems.

rest of the A -body system. The relative distance or momentum of the two clusters point here towards the i -nucleon cluster. This operation can be repeated to form states with a special subclustering. The graphical representation given in the table should clarify the clusters involved. Since we are going to obtain the basis states recursively starting from $A = 3$, A -body cluster states are labeled by the index of the $(A-x)$ N-clusters. The contributing indices are given in the third column. The number of particles of the subclusters is here given as a subscript. We assume that the complete state and the clusters are antisymmetrized which is not the case anymore for the states that explicitly single out clusters. This implies that more states are required to cover the physical Hilbert space completely. The last column of the table gives first estimates of the relations of the dimensionalities.

It is now the aim to express the completely antisymmetric states in terms of $|\alpha^{*(1)}\rangle$. In the first step, we therefore need to obtain the antisymmetrization operator \mathcal{A} in this basis. Assuming antisymmetry for the $(A-1)$ -nucleon system, the matrix of \mathcal{A} for A nucleons can be written in terms of the transposition operator of the outer two nucleons $\mathcal{P}_{A-1,A}$ as

$$\langle \alpha^{*(1)} | \mathcal{A} | \beta^{*(1)} \rangle = \frac{1}{A} \langle \alpha^{*(1)} | (\mathbb{1} - (A-1) \mathcal{P}_{A-1,A}) | \beta^{*(1)} \rangle. \quad (13)$$

The antisymmetric A -body states are eigenstates of \mathcal{A} for the eigenvalue $\lambda = 1$, e.g. are solutions of

$$\langle \alpha^{*(1)} | \mathcal{A} | \gamma^{*(1)} \rangle \langle \gamma^{*(1)} | \beta \rangle = \lambda \langle \alpha^{*(1)} | \beta \rangle = \langle \bullet \circ | \circ \rangle. \quad (14)$$

Here, the graphical representation of the states is added to simplify the notation and a sum over $\gamma^{*(1)}$ -states is implied. The matrix elements $\langle \bullet \circ | \circ \rangle$ are the well-known coefficients of fractional parentage (cfp) [29] which define the antisymmetric A -body state in terms of antisymmetric $(A-1)$ -body states in relative motion with respect to the A -th nucleon. We will obtain these states by diagonalization of \mathcal{A} . The problem is therefore reduced to the calculations of the matrix $\langle \alpha^{*(1)} | \mathcal{A} | \gamma^{*(1)} \rangle$. To this aim, we need to explicitly define the coupling scheme for states $|\alpha^{*(1)}\rangle$ given by

$$|\alpha^{*(1)}\rangle = |\alpha_{A-1} \ n_A (l_A s_A) I_A t_A; (J_{A-1} I_A) J (T_{A-1} t_A) T\rangle. \quad (15)$$

The states are based on complete antisymmetrized states $|\alpha_{A-1}\rangle$ with well defined total angular momentum J_{A-1} and isospin T_{A-1} and total HO energy quantum number \mathcal{N}_{A-1} . Note that we dropped the last quantum number in Eq. (15) to simplify the notation. The motion of the A -th nucleon is given by its HO quantum number n_A , orbital angular momentum l_A , spin $s_A = \frac{1}{2}$, total angular momentum I_A and isospin $t_A = \frac{1}{2}$. In order to end up with a well-defined total angular momentum J and isospin T of the A -body system, we finally couple the individual angular momenta and isospins as indicated.

The antisymmetrization operator is given by $\mathcal{P}_{A-1,A}$. In the next step, we therefore need to use the known cfp of the $(A-1)$ -nucleon system to disentangle the $(A-1)$ -th nucleon from the antisymmetric cluster. We end up with states

$$|(\alpha^{*(1)})^{*(1)}\rangle = |\alpha_{A-1}^{*(1)} \ n_A (l_A s_A) I_A t_A; (J_{A-1} I_A) J (T_{A-1} t_A) T\rangle. \quad (16)$$

or more explicitly by reinserting the definition Eq. (15)

$$|(\alpha^{*(1)})^{*(1)}\rangle = |\alpha_{A-2} \ n_{A-1} (l_{A-1} s_{A-1}) I_{A-1} t_{A-1}, \ n_A (l_A s_A) I_A t_A; ((J_{A-2} I_{A-1}) J_{A-1} I_A) J ((T_{A-2} t_{A-1}) T_{A-1} t_A) T\rangle = |\circ \circ \bullet\rangle. \quad (17)$$

Table 2 Identification of quantum numbers in states of Eq. (17) to the ones of the permutation operators in Eqs.(11) and (12). Given are only relations to the quantum numbers of Eq. (3) since the relation to Eq. (7) is a simple generalization.

n_{12}	n_3	l_{12}	s_1	s_2
n_{A-1}	n_A	l_{A-1}	J_{A-2}	$\frac{1}{2}$
J_{12}	l_3	s_3	I_3	J
J_{A-1}	l_A	$\frac{1}{2}$	I_A	J
t_1	t_2	T_{12}	t_3	T
T_{A-2}	$\frac{1}{2}$	T_{A-1}	$\frac{1}{2}$	T
S_{12}				
sum				

Again, the graphical representation is given to simplify the expression. The complete coupling scheme will however be important to explicitly obtain the matrix element of $\mathcal{P}_{A-1,A}$. The directions of the momenta (or coordinates) are given in the more detailed Fig. 2. In order to match the states of Eqs. (3) and (7) with the ones of Eq. (17), we first identify the clusters 2 and 3 with the nucleons $A-1$ and A . Comparing the directions given in Fig. 1 and 2, it is obvious that the position vectors of the spectator agree with the one of A -th nucleon, but the relative positions of the $(A-2)$ -nucleon cluster and the $(A-1)$ -th nucleon are opposite implying additional phases $(-)^{l_{A-1}}$ for each of the states. The coupling of the angular momentum quantum numbers of the subsystem is also different to the general three cluster expression. We need an additional $6j$ coefficient and extra phase to recouple from

$$(J_{A-2} (l_{A-1} s_{A-1}) I_{A-1}) J_{A-1} \quad \text{to} \quad (l_{A-1} (J_{A-2} s_{A-1}) S_{12}) J_{A-1} \quad . \quad (18)$$

S_{12} is a new quantum number we need to sum over. Its name is chosen to match Eq. (3), for Eq. (7) S_{13} is more natural.

After this recoupling the quantum numbers can be identified to the ones of Eq. (11) as shown in Table 2 leading to the matrix element of the permutation operator

$$\begin{aligned}
\langle (\gamma^{*(1)})^{*(1)} | \mathcal{P}_{A-1,A} | (\delta^{*(1)})^{*(1)} \rangle &= \langle \text{diagram} | \text{diagram} \rangle = (-1)^{2J_{A-2} + I_{A-1}^\delta + T_{A-1}^\delta + l_A^\delta + I_{A-1}^\gamma + T_{A-1}^\gamma + l_A^\gamma} \\
&\times \hat{I}_{A-1}^\gamma \hat{J}_{A-1}^\gamma \hat{T}_{A-1}^\gamma \hat{I}_A^\gamma \hat{I}_{A-1}^\delta \hat{J}_{A-1}^\delta \hat{T}_{A-1}^\delta \hat{I}_A^\delta \sum_{S_{12} S_{13}} \hat{S}_{13}^2 \hat{S}_{12}^2 \left\{ \begin{matrix} J_{A-2} & \frac{1}{2} & S_{13} \\ l_{A-1}^\gamma & J_{A-1}^\gamma & I_{A-1}^\gamma \end{matrix} \right\} \left\{ \begin{matrix} J_{A-2} & \frac{1}{2} & S_{12} \\ l_{A-1}^\delta & J_{A-1}^\delta & I_{A-1}^\delta \end{matrix} \right\} \\
&\times \sum_{LS} \hat{L}^2 \hat{S}^2 \left\{ \begin{matrix} \frac{1}{2} & J_{A-2} & S_{13} \\ \frac{1}{2} & S & S_{12} \end{matrix} \right\} \left\{ \begin{matrix} \frac{1}{2} & T_{A-2} & T_{A-1}^\gamma \\ \frac{1}{2} & T & T_{A-1}^\delta \end{matrix} \right\} \left\{ \begin{matrix} l_{A-1}^\gamma & S_{13} & J_{A-1}^\gamma \\ l_A^\gamma & \frac{1}{2} & I_A^\gamma \end{matrix} \right\} \left\{ \begin{matrix} l_{A-1}^\delta & S_{12} & J_{A-1}^\delta \\ l_A^\delta & \frac{1}{2} & I_A^\delta \end{matrix} \right\} \\
&\times \langle n_{A-1}^\gamma l_{A-1}^\gamma, n_A^\gamma l_A^\gamma : L | n_{A-1}^\delta l_{A-1}^\delta, n_A^\delta l_A^\delta : L \rangle_{d=\frac{1}{A(A-2)}} \quad . \quad (19)
\end{aligned}$$

The left and right hand side states are labeled by superscripts γ and δ . We omitted these labels for quantum numbers that are conserved. Kronecker δ 's for these quantum numbers are implied. To complete the antisymmetrization operator of Eq. (13), we only need to use the cfp obtained before for the $(A-1)$ N-system to relate the $(\gamma^{*(1)})^{*(1)}$ to $\beta^{*(1)}$ states

$$\langle (\delta^{*(1)})^{*(1)} | \beta^{*(1)} \rangle = \langle \text{diagram} | \text{diagram} \rangle = \delta_{\text{spectator}} \langle \text{diagram} | \text{diagram} \rangle_{A-1} = \delta_{\text{spectator}} \langle \delta^{*(1)} | \beta \rangle_{A-1} \quad (20)$$

The Kronecker symbol $\delta_{\text{spectator}}$ represents the conservation of all spectator quantum numbers, the total angular momentum, isospin and HO energy quantum numbers for the $(A-1)$ -body subsystem and the A -body system. The permutation operator of Eq. (13) can then be represented by

$$\langle \alpha^{*(1)} | \mathcal{P}_{bc} | \beta^{*(1)} \rangle = \langle \alpha^{*(1)} | (\gamma^{*(1)})^{*(1)} \rangle \langle (\gamma^{*(1)})^{*(1)} | \mathcal{P}_{A-1,A} | (\delta^{*(1)})^{*(1)} \rangle \langle (\delta^{*(1)})^{*(1)} | \beta^{*(1)} \rangle$$

Table 3 Dimensions of selected sets of α , $\alpha^{*(1)}$, $(\alpha^{*(1)})^{*(1)}$ and $\alpha^{*(A-2)}$ states for blocks with given total angular momentum, isospin and HO energy quantum number for an A -nucleon system.

A	J	T	\mathcal{N}	$\dim(\alpha)$	$\dim(\alpha^{*(1)})$	$\dim((\alpha^{*(1)})^{*(1)})$	$\dim(\alpha^{*(A-2)})$
4	0	0	10	217	791	2373	1225
4	0	0	12	417	1551	4648	2380
4	4	0	12	2123	8370	25110	–
4	4	1	12	3104	12516	37626	–
7	1/2	1/2	7	1269	9957	65369	32190
7	1/2	1/2	9	8963	67453	429132	212318
7	5/2	1/2	9	18839	142535	910342	–
7	5/2	3/2	9	16629	130896	861394	–

$$= \langle \bullet \circ \bullet | \bullet \circ \bullet \rangle \langle \bullet \circ \bullet | \bullet \circ \bullet \rangle \langle \bullet \circ \bullet | \bullet \circ \bullet \rangle \langle \bullet \circ \bullet | \bullet \circ \bullet \rangle \quad (21)$$

where a sum over intermediate states is implied. Because the total angular momentum J , isospin T and HO energy quantum number \mathcal{N} is conserved by $\langle \alpha^{*(1)} | \mathcal{P}_{bc} | \beta^{*(1)} \rangle$, the antisymmetrized states can be obtained for each J , T and \mathcal{N} separately. To this aim, we implemented a parallelized code that generates the antisymmetrization matrix elements of Eq. (13) for each block J , T and \mathcal{N} and performs a diagonalization using the parallelized eigenvector packages SCALAPACK [30] and ELPA [31]. The starting point of the recursive procedure is the $A = 3$ system where we impose antisymmetry of the (12)-subsystem via the condition $(-1)^{l_{12}+S_{12}+T_{12}}$. Here, we use the basis set Eq. (3) directly to represent the antisymmetrized states of the three nucleons without further recoupling. Based on the diagonalization of the permutation operator as given in Eq. (12), antisymmetrized states are found that are then used to recursively proceed to $A > 3$.

Explicit calculations confirmed that the antisymmetrization operator \mathcal{A} has only two eigenvalues $\lambda = 0$ and 1. The dimension of the eigenspace for $\lambda = 1$ is approximately by a factor $\frac{1}{A}$ smaller than the total dimensionality of the space spanned by $|\alpha^{*(1)}\rangle$. The normalized eigenvectors are the cfp. We note that fully antisymmetrized states (and eigenvalues $\lambda = 0, 1$) are only obtained when the complete block of intermediate states for J , T and \mathcal{N} was included. In this first study, we also included all states of the $(A-2)$ N-subsystem that can be combined with the two outer nucleons to J , T and \mathcal{N} . The dimensions of selected sets of α , $\alpha^{*(1)}$ and $(\alpha^{*(1)})^{*(1)}$ states are given in Table 3. The sets generated so far are tabulated in Appendix B. They will be made available in the machine independent HDF5 format [32].

3 2N+(A-2)N states for 2N operators

For the representation of two-nucleon operators as for example the NN interaction, the complete antisymmetrized states are not suitable. The most efficient way to obtain matrix elements for these operators is to change to a basis that singles out two nucleons from the A -nucleon system. Following the notation of Table 1, such states are given by $|\alpha^{*(A-2)}\rangle$. It is the aim of this section to calculate the overlap $\langle \alpha | \beta^{*(A-2)} \rangle$. Again these transition coefficients will be independent of the HO frequency and



Fig. 3 Left hand side: more detailed definition of $|\alpha^{*(A-2)}\rangle$ states including the direction of momenta. Right hand side: the same for $|\left(\alpha^{*(1)}\right)^{*(1)}\rangle$ states.

Table 4 Left hand side: Identification of quantum numbers of $|\alpha^{*(A-2)}\rangle$ states to the ones of the coordinate transformation in Eq.(11) used to obtain the transitions to $2N+(A-2)$ states. Right hand side: the same for $|\left(\alpha^{*(1)}\right)^{*(1)}\rangle$ states.

n_{12}	n_3	l_{12}	s_1	s_2
n_{12}	n_λ	l_{12}	$\frac{1}{2}$	$\frac{1}{2}$
J_{12}	l_3	s_3	I_3	J
J_{12}	λ	J_{A-2}	I_λ	J
t_1	t_2	T_{12}	t_3	T
$\frac{1}{2}$	$\frac{1}{2}$	T_{12}	T_{A-2}	T
S_{12}				
S_{12}				

n_{13}	n_2	l_{13}	s_1	s_2
n_{A-1}	n_A	l_{A-1}	$\frac{1}{2}$	$\frac{1}{2}$
J_{13}	l_2	s_3	I_2	J
J_{A-1}	l_A	J_{A-2}	I_A	J
t_1	t_2	T_{13}	t_3	T
$\frac{1}{2}$	$\frac{1}{2}$	T_{A-1}	T_{A-2}	T
S_{13}				
sum				

will conserve total A -body J , T and \mathcal{N} . Since the two-body states are directly linked to the matrix elements of any two-nucleon operator, it will be straightforward to apply these operator to any A -body state once the transition matrix elements are known.

Explicitly, the $|\alpha^{*(A-2)}\rangle$ states are given by

$$|\alpha^{*(A-2)}\rangle = |\alpha_{12} n_\lambda \lambda \alpha_{A-2}; ((l_{12} (s_1 s_2) S_{12}) J_{12} (\lambda J_{A-2}) I_\lambda) J ((t_1 t_2) T_{12} T_{A-2}) T \rangle \quad (22)$$

The state of the two-nucleon subsystem is labeled here with α_{12} . As usual this combined label corresponds to the HO quantum number n_{12} , the orbital angular momentum l_{12} and spin S_{12} that are coupled to the total angular momentum J_{12} and the total isospin T_{12} of the two-nucleon subsystem. The relative motion of this cluster with respect to the $(A-2)N$ rest system is described by the HO quantum number n_λ and the orbital angular momentum λ . The quantum numbers α_{A-2} , J_{A-2} and T_{A-2} have already been defined above. In order to be able to define the total angular momentum, one intermediate quantum number I_λ is necessary, which is given here by coupling λ and J_{A-2} . Note that the conventions for the direction of momenta and orderings of couplings correspond indeed to $|\alpha^{*(A-2)}\rangle$ as can be seen in Fig. 3 and not, as one might naively expect, to $|\alpha^{*(2)}\rangle$. For shorter notation, we label the two nucleons separated out with number 1 and 2 here, but whenever we are referring to $|\left(\alpha^{*(1)}\right)^{*(1)}\rangle$ we keep labeling them nucleon $A-1$ and A as done in the previous section.

The transition can be done most easily in two steps which mostly involve matrix elements already known. We first use the cfp $\langle \alpha | \gamma^{*(1)} \rangle = \langle \text{circle} | \text{circle} \bullet \rangle$ obtained by solving Eq. (14) and then

$\langle \gamma^{*(1)} | \left(\delta^{*(1)}\right)^{*(1)} \rangle = \langle \text{circle} \bullet | \bullet \text{circle} \rangle$ that were already involved in the definition of the antisymmetrization operator Eq. (21). The final step, the transition $\langle \left(\delta^{*(1)}\right)^{*(1)} | \beta^{*(A-2)} \rangle = \langle \bullet \text{circle} | \bullet \text{circle} \bullet \rangle$, is new but

can also be traced back to the general change of three-body coordinates defined in Eq. (11). We identify this time the clusters 1 and 2 with the nucleons $A-1$ and A and the $(A-2)N$ -subsystem with cluster 3. For this choice, the position vectors of the spectator agree with the directions used in Fig. 1 as can be easily seen by comparing to Fig. 3. In order to match the $|\left(\alpha^{*(1)}\right)^{*(1)}\rangle$ states to the general expressions a recoupling is necessary again resulting in a sum over an intermediate spin quantum number S_{13} , a

6j-coefficient and phases which differ from the ones in the previous section because the different identification of clusters used in $|\left(\alpha^{*(1)}\right)^{*(1)}\rangle$ here and in the previous section requires an opposite order for the coupling of J_{A-2} and $\frac{1}{2}$ to S_{13} in order to match to Eq. (11). Then the quantum numbers can be identified as summarized in Table 4. Altogether, we find

$$\begin{aligned}
& \langle (\delta^{*(1)})^{*(1)} | \beta^{*(A-2)} \rangle \\
&= \langle \text{diagram} \rangle \\
&= (-1)^{3J_{A-2}+2T_{A-2}+I_{A-1}^\delta+l_{A-1}^\delta+l_A^\delta+S_{12}^\beta+T_{12}^\beta+\lambda^\beta} \\
&\quad \times \hat{I}_{A-1}^\delta \hat{J}_{A-1}^\delta \hat{T}_{A-1}^\delta \hat{I}_A^\delta \hat{S}_{12}^\beta \hat{J}_{12}^\beta \hat{T}_{12}^\beta \hat{I}_\lambda^\beta \\
&\quad \times \sum_{S_{13}} (-1)^{S_{13}} \hat{S}_{13}^2 \left\{ \begin{matrix} J_{A-2} & \frac{1}{2} & S_{13} \\ l_{A-1}^\delta & J_{A-1}^\delta & I_{A-1}^\delta \end{matrix} \right\} \\
&\quad \times \sum_{LS} \hat{L}^2 \hat{S}^2 \left\{ \begin{matrix} \frac{1}{2} & \frac{1}{2} & S_{12}^\beta \\ J_{A-2} & S & S_{13} \end{matrix} \right\} \left\{ \begin{matrix} \frac{1}{2} & \frac{1}{2} & T_{12}^\beta \\ T_{A-2} & T & T_{A-1}^\delta \end{matrix} \right\} \\
&\quad \times \left\{ \begin{matrix} l_{A-1}^\delta & S_{13} & J_{A-1}^\delta \\ l_A^\delta & \frac{1}{2} & I_A^\delta \\ L & S & J \end{matrix} \right\} \left\{ \begin{matrix} l_{12}^\beta & S_{12}^\beta & J_{12}^\beta \\ \lambda^\beta & J_{A-2} & I_\lambda^\beta \\ L & S & J \end{matrix} \right\} \\
&\quad \times \langle n_{A-1}^\delta l_{A-1}^\delta, n_A^\delta l_A^\delta : L | n_{12}^\beta l_{12}^\beta, n_\lambda^\beta \lambda^\beta : L \rangle_{d=\frac{A-2}{A}} . \tag{23}
\end{aligned}$$

for this third matrix element.

Based on these three ingredients, the transition to $|\beta^{*(A-2)}\rangle$ states is obtained by

$$\begin{aligned}
\langle \alpha | \beta^{*(A-2)} \rangle &= \langle \text{diagram} \rangle \\
&= \langle \alpha | \gamma^{*(1)} \rangle \langle \gamma^{*(1)} | (\delta^{*(1)})^{*(1)} \rangle \langle (\delta^{*(1)})^{*(1)} | \beta^{*(A-2)} \rangle \\
&= \langle \text{diagram} \rangle \langle \text{diagram} \rangle \langle \text{diagram} \rangle \tag{24}
\end{aligned}$$

where summations over the intermediate states is implied. This has been implemented in two steps. We decided to first perform the summation over $\gamma^{*(1)}$, store the intermediate result in core memory and then proceed to the $(\delta^{*(1)})^{*(1)}$ summation. In Table 3, we also give the dimensions for $\alpha^{*(A-2)}$ states for a few selected blocks. The transition matrix element will be made publicly available in HDF5 format. The sets generated so far are also tabulated in Appendix B.

4 3N+(A-3)N states for 3N operators

Although we have not used them in this first application, it will be important in future to apply also 3N operators, e.g. to take 3N interactions into account. As can be seen below, the calculation of the pertinent transition coefficients can be done in three steps involving four kinds of matrix elements. Therefore, the calculation is not a direct extension of the 2N+(A-2)N transitions discussed in the previous section. We note however that further extensions towards 4N, 5N, ... operators can be done using the same three steps as outlined now for the 3N case. Also for this reason, we consider it interesting to explicitly give our results for the 3N+(A-3)N transitions here.

For the application of the 3N operators, we define states

$$|\alpha^{*(A-3)}\rangle = |\alpha_3 \ n_\lambda \lambda \ \alpha_{A-3}; (J_3 \ (\lambda J_{A-3}) \ I_\lambda) \ J \ (T_3 \ T_{A-3}) \ T \rangle \tag{25}$$

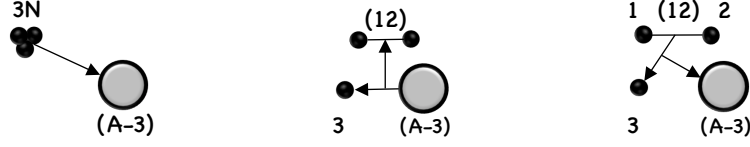


Fig. 4 Left hand side: more detailed definition of $|\alpha^{*(A-3)}\rangle$ states including the direction of momenta. Middle: the same for $|\left(\alpha^{*(1)}\right)^{*(2)}\rangle$ states. Right hand side: the same for $|\left(\alpha^{*(1)}\right)^{*(A-3)}\rangle$ states.

Table 5 Left hand side: Identification of quantum numbers of $|\left(\alpha^{*(1)}\right)^{*(A-3)}\rangle$ states to the ones of the coordinate transformation in Eq.(11) used to obtain the transitions to $3N+(A-3)$ states. Right hand side: the same for $|\left(\alpha^{*(1)}\right)^{*(2)}\rangle$ states.

n_{12}	n_3	l_{12}	s_1	s_2	n_{13}	n_2	l_{13}	s_1	s_2
n_3	n_λ	l_3	$\frac{1}{2}$	J_{12}	n_{A-2}	n_λ	l_{A-2}	$\frac{1}{2}$	J_{12}
J_{12}	l_3	s_3	I_3	J	J_{13}	l_2	s_3	I_2	J
J_3	λ	J_{A-3}	I_λ	J	J_{A-2}	λ	J_{A-3}	I_λ	J
t_1	t_2	T_{12}	t_3	T	t_1	t_2	T_{13}	t_3	T
$\frac{1}{2}$	T_{12}	T_3	T_{A-3}	T	$\frac{1}{2}$	T_{12}	T_{A-2}	T_{A-3}	T
S_{12}					S_{13}				
S_3					S_{A-2}				

which single out a three-nucleon cluster. The state of the three-nucleon subsystem is labeled here with α_3 . This state is one of the antisymmetrized $3N$ states obtained by diagonalizing the $3N$ system for a given total $3N$ angular momentum J_3 , isospin T_3 and HO quantum number \mathcal{N}_3 . The states are therefore only meaningfully defined in conjunction with an *a priori* given set of cfp for the $3N$ system. The relative motion of this cluster with respect to the $(A-3)N$ -subsystem is described by the HO quantum number n_λ and the orbital angular momentum λ . The quantum numbers α_{A-3} , J_{A-3} and T_{A-3} label the antisymmetrized state of the $(A-3)N$ -cluster. Again, in order to be able to define the total angular momentum, one intermediate quantum number I_λ is necessary, which is given here by coupling λ and J_{A-3} . The conventions for the direction of momenta can be read off from the left hand side of Fig. 4.

To define the transition matrix elements $\langle \alpha | \beta^{*(A-3)} \rangle = \langle \text{grey circle} | \text{three dots with arrows} \rangle$, we need to introduce two further sets of intermediate states:

$$\begin{aligned}
 |(\alpha^{*(1)})^{*(2)}\rangle &= |\alpha_{A-2}^{*(1)} n_\lambda \lambda \alpha_{12}; \\
 &\quad ((J_{A-3} (l_{A-2} s_3) I_{A-2}) J_{A-2} (\lambda J_{12}) I_\lambda) J ((T_{A-3} t_3) T_{A-2} T_{12}) T) \\
 |(\alpha^{*(1)})^{*(A-3)}\rangle &= |\alpha_3^{*(1)} n_\lambda \lambda \alpha_{A-3}; \\
 &\quad ((J_{12} (l_3 s_3) I_3) J_3 (\lambda J_{A-3}) I_\lambda) J ((T_{12} t_3) T_3 T_{A-3}) T)
 \end{aligned} \tag{26}$$

which are also depicted in Fig. 4. Three of the four involved matrix elements are already known from previous calculations. In the first step, we will need the transition coefficients to $2N+(A-2)N$ states $\langle \alpha | \gamma^{*(A-2)} \rangle = \langle \text{grey circle} | \text{two dots with arrows} \rangle$ and, in the final step, cfp for the $3N$ system $\langle (\epsilon^{*(1)})^{*(A-3)} | \beta^{*(A-3)} \rangle = \langle \text{three dots with arrows} | \text{grey circle} \rangle$. Also the matrix elements $\langle \gamma^{*(A-2)} | (\delta^{*(1)})^{*(2)} \rangle = \langle \text{two dots with arrows} | \text{two dots with arrows} \rangle$ are given by the known cfp of the $(A-2)N$ -system. The only new ingredient $\langle (\delta^{*(1)})^{*(2)} | (\epsilon^{*(1)})^{*(A-3)} \rangle = \langle \text{two dots with arrows} | \text{three dots with arrows} \rangle$ can again be traced back to the general change of three body coordinates defined in Eq. (11). Comparing the coordinates depicted in middle and right of Fig. 4 with the general coordinates of Fig. 1, one easily identifies clusters 1, 2 and 3 with the third nucleon, the $2N$ -cluster and the $(A-3)N$ -subsystem. Also the direction of the coordinates agree in this case with the general ones. But the coupling scheme

of both kinds of states, $|(\alpha^{*(1)})^{*(2)}\rangle$ and $|(\alpha^{*(1)})^{*(A-3)}\rangle$, do not fit to the general expression. For the $|(\alpha^{*(1)})^{*(2)}\rangle$, we therefore recouple the angular momenta of the $(A-2)$ N-subsystem from

$$(J_{A-3} (l_{A-2} s_3) I_{A-2}) J_{A-2} \quad \text{to} \quad (l_{A-2} (s_3 J_{A-3}) S_{A-2}) J_{A-2} \quad (27)$$

whereby introducing the new intermediate spin quantum number S_{A-2} . Similarly, the original coupling of the $|(\epsilon^{*(1)})^{*(A-3)}\rangle$ states has to be recoupled from

$$(J_{12} (l_3 s_3) I_3) J_3 \quad \text{to} \quad (l_3 (s_3 J_{12}) S_3) J_3 \quad (28)$$

where S_3 was introduced as a new spin quantum number. Both recouplings lead to $6j$ -coefficients and phases. Then the quantum numbers can be matched to the ones of Eq. (11) as shown in Table 5. The complete expression then reads

$$\begin{aligned} \langle (\delta^{*(1)})^{*(2)} | (\epsilon^{*(1)})^{*(A-3)} \rangle &= \langle \text{---} \bullet \circ \text{---} | \text{---} \bullet \circ \text{---} \rangle \\ &= (-1)^{3J_{A-3} + l_{A-2}^\delta + I_{A-2}^\delta + 2T_{A-2}^\delta + l_3^\epsilon + I_3^\epsilon + 1 + J_{12} + \lambda^\delta + \lambda^\epsilon} \\ &\quad \times \hat{I}_{A-2}^\delta \hat{J}_{A-2}^\delta \hat{T}_{A-2}^\delta \hat{I}_\lambda^\delta \hat{I}_3^\epsilon \hat{T}_3^\epsilon \hat{J}_3^\epsilon \hat{I}_\lambda^\epsilon \\ &\quad \times \sum_{S_{A-2} S_3} (-1)^{S_{A-2} + S_3} \hat{S}_{A-2} \hat{S}_3^2 \\ &\quad \times \left\{ \begin{matrix} J_{A-3} & \frac{1}{2} & S_{A-2} \\ l_{A-2}^\delta & J_{A-2}^\delta & I_{A-2}^\delta \end{matrix} \right\} \left\{ \begin{matrix} J_{12} & \frac{1}{2} & S_3 \\ l_3^\epsilon & J_3^\epsilon & I_3^\epsilon \end{matrix} \right\} \\ &\quad \times \sum_{LS} \hat{L}^2 \hat{S}^2 \left\{ \begin{matrix} J_{12} & \frac{1}{2} & S_3 \\ J_{A-3} & S & S_{A-2} \end{matrix} \right\} \left\{ \begin{matrix} T_{12} & \frac{1}{2} & T_3^\epsilon \\ T_{A-3} & T & T_{A-2}^\delta \end{matrix} \right\} \\ &\quad \times \left\{ \begin{matrix} l_{A-2}^\delta & S_{A-2} & J_{A-2}^\delta \\ \lambda^\delta & J_{12} & I_\lambda^\delta \\ L & S & J \end{matrix} \right\} \left\{ \begin{matrix} l_3^\epsilon & S_3 & J_3^\epsilon \\ \lambda^\epsilon & J_{A-3} & I_\lambda^\epsilon \\ L & S & J \end{matrix} \right\} \\ &\quad \times \langle n_{A-2}^\delta l_{A-2}^\delta, n_\lambda^\delta \lambda^\delta : L | n_3^\epsilon l_3^\epsilon, n_\lambda^\epsilon \lambda^\epsilon : L \rangle_{d=\frac{2(A-3)}{A}} \end{aligned} \quad (29)$$

We note that the extension to $4N$ -($A-4$) N transitions will only require straightforward changes of this relation. Based on these three ingredients, the transition to $|\beta^{*(A-3)}\rangle$ states is obtained by

$$\begin{aligned} \langle \alpha | \beta^{*(A-3)} \rangle &= \langle \text{---} \bullet \circ \text{---} | \text{---} \bullet \circ \text{---} \rangle \\ &= \langle \alpha | \gamma^{*(A-2)} \rangle \langle \gamma^{*(A-2)} | (\delta^{*(1)})^{*(2)} \rangle \langle (\delta^{*(1)})^{*(2)} | (\epsilon^{*(1)})^{*(A-3)} \rangle \langle (\epsilon^{*(1)})^{*(A-3)} | \beta^{*(A-3)} \rangle \\ &= \langle \text{---} \bullet \circ \text{---} | \text{---} \bullet \circ \text{---} \rangle \langle \text{---} \bullet \circ \text{---} | \text{---} \bullet \circ \text{---} \rangle \langle \text{---} \bullet \circ \text{---} | \text{---} \bullet \circ \text{---} \rangle \langle \text{---} \bullet \circ \text{---} | \text{---} \bullet \circ \text{---} \rangle \langle \text{---} \bullet \circ \text{---} | \text{---} \bullet \circ \text{---} \rangle \end{aligned} \quad (30)$$

where again sums over intermediate states are implied. Our implementation generates the complete expression in three steps where the results dependent on the intermediate quantum numbers. As can be seen from Table 1, the size of these sets of intermediate states are orders of magnitude larger than the set of completely antisymmetrized A -body states implying not only more floating point operations but also larger memory requirements. The parallelization on a distributed memory massively parallel computer therefore required a compromise of most efficient memory usage and minimalization of communication between the processes. The details of the technical implementation are discussed in more detail in [33]. We stress again that an extension to more complex operators can be done using the same algorithms in future.

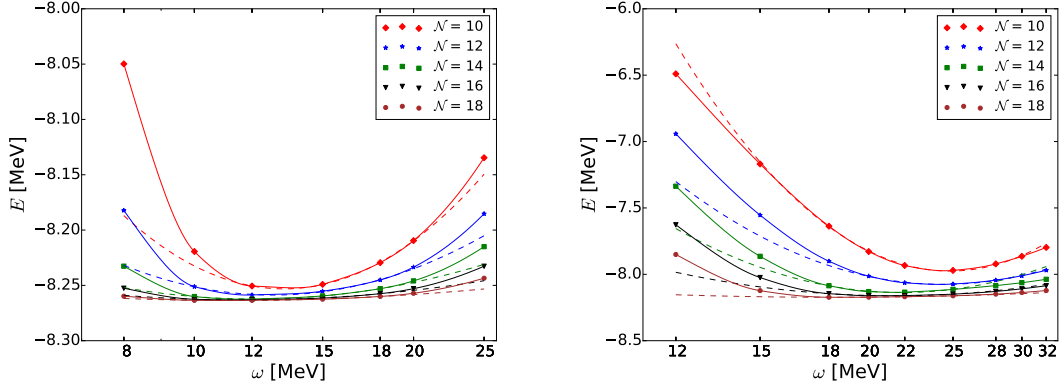


Fig. 5 ω -dependence of the ${}^3\text{H}$ binding energy for $\lambda = 1.5 \text{ fm}^{-1}$ (left) and $\lambda = 2.5 \text{ fm}^{-1}$ (right). Results for different model space sizes can be distinguished by the different markers and colors. The solid lines are added to guide the eye, the dashed lines are obtained using Eq. (33).

5 Results

As a first application of the cfp and transition coefficients, we are now presenting binding energies for light nuclei based on these Jacobi HO states. For this test, we only use NN interactions. In order to be able to obtain converged results, we rely on SRG evolved interactions [24] starting from the chiral interaction at next-to-next-to-next-to-leading order (N^3LO) from the Idaho group [34] considering NN partial waves up to $J_{\text{NN}}^{\text{max}} = 6$. The charge dependence of the nuclear force is taken into account by building an averaged NN interaction as outlined in [35]. The relative weight of proton-proton (pp), neutron-neutron (nn) and neutron-proton (np) interactions in isospin $T_{12} = 1$ states thereby depend on the nucleus considered. For pp and nn interactions, we added the electromagnetic interactions of AV18 [36].

For the solution of the Schrödinger equation and taking only NN interactions into account, we rewrite the matrix elements of the Hamiltonian in the antisymmetrized A -nucleon basis $|\alpha\rangle$ as

$$\langle \alpha | H_A | \beta \rangle = \langle \alpha | \gamma^{*(A-2)} \rangle \langle \gamma^{*(A-2)} | \sum_{i < j = 1}^A H_{ij} | \delta^{*(A-2)} \rangle \langle \delta^{*(A-2)} | \beta \rangle . \quad (31)$$

The coefficients $\langle \alpha | \gamma^{*(A-2)} \rangle$ are known from the previous sections, independent of the HO frequency ω and conserve total J, T and \mathcal{N} . The two-nucleon matrix elements can be simplified making use of the identity of the nucleons

$$\langle \gamma^{*(A-2)} | \sum_{i < j = 1}^A H_{ij} | \delta^{*(A-2)} \rangle = \delta_{(\mathcal{N}, J, T) \gamma_{A-2} (\mathcal{N}, J, T) \delta_{A-2}} \binom{A}{2} \langle \gamma_{12} | \left(\frac{2}{A} T_{12} + V_{12} \right) | \delta_{12} \rangle . \quad (32)$$

It is convenient to express the relative kinetic energy in terms of an NN operator. This matrix elements conserves J and T in our approximation. It will however not conserve \mathcal{N} . Nevertheless, all quantum numbers of the $(A-2)\text{N}$ -subsystem are conserved as indicated by the Kronecker δ symbols. As usual, the NN interaction is diagonal in J_{12} and T_{12} . Therefore, the application of H_A on an arbitrary A -body state can be separated in three steps that only evolve rather low dimensional operations. The use of Jacobi coordinates further reduces the dimensionality since the problem can be solved for each J and T independently. Therefore, once the cfp and transition coefficients are known, the calculations are much simpler and can be done quickly. In the following, we therefore map out the complete dependence on the HO frequency ω of the energy of each state for all model space size defined by the maximal HO energy \mathcal{N} .

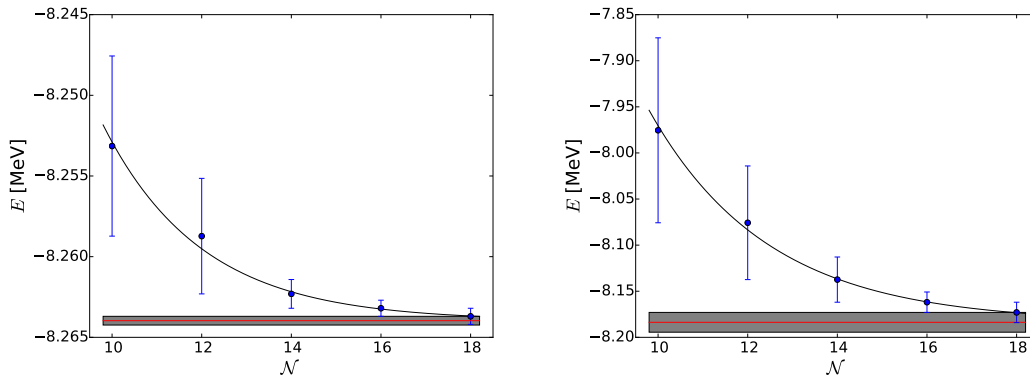


Fig. 6 \mathcal{N} -dependence of the ${}^3\text{H}$ binding energy for $\lambda = 1.5 \text{ fm}^{-1}$ (left) and $\lambda = 2.5 \text{ fm}^{-1}$ (right). The black line is obtained using Eq. (34). The result of the exponential extrapolation is indicated by the red line. The shaded area indicates the estimated uncertainty of the final result which is given by the difference of the result for the largest model space and the exponential extrapolation.

5.1 Extrapolation procedure for the example of ${}^3\text{H}$

We found that in most cases the ω -dependence around the optimal frequency ω_0 can be well described by the ansatz

$$E_b(\omega) = E_{\mathcal{N}} + \kappa (\log(\omega) - \log(\omega_{opt}))^2 . \quad (33)$$

By a simple fit, the parameters $E_{\mathcal{N}}$, ω_0 and κ are extracted from the results for a given model space size \mathcal{N} (in a limited region around ω_0). As an example, we show the ω -dependence as solid lines for the case of ${}^3\text{H}$ in Fig. 5 for two different SRG cutoffs $\lambda = 1.5 \text{ fm}^{-1}$ and $\lambda = 2.5 \text{ fm}^{-1}$. Different lines correspond to different model space sizes. The result of the fit to Eq. (33) is also shown by the dashed lines. As expected the results become less ω dependent for larger model spaces. It is also clearly seen that the convergence is much faster for smaller λ . For this small system, it is still possible to obtain converged results for $\lambda = 2.5 \text{ fm}^{-1}$, this will however not be possible anymore for the more complex nuclei. For $\lambda = 1.5 \text{ fm}^{-1}$, the convergence is fast enough that we will also be able to present converged numbers for p -shell nuclei for this first application. Around the optimal $\omega = \omega_0$ at the minimum, Eq. (33) is able to reproduce the ω -dependence very well. The agreement of the calculations with the results even improves for larger model spaces. Therefore, we will extract our final result for a given model space using the fit result $E_{\mathcal{N}}$.

Fig. 6 summarizes these results again for ${}^3\text{H}$ and $\lambda = 1.5 \text{ fm}^{-1}$ and $\lambda = 2.5 \text{ fm}^{-1}$. In order to extract the converged binding energy from the \mathcal{N} -dependence, we assume a simple exponential dependence

$$E_{\mathcal{N}} = E_{\infty} + A e^{-b\mathcal{N}} . \quad (34)$$

We note that other effective field theory motivated extrapolation schemes have been discussed in [39; 40]. They should be employed in forthcoming publications. But for our purpose here, the exponential interpolation was sufficiently accurate to determine the final binding energies. In order to determine E_{∞} , A and b , we first assign an uncertainty estimate to each $E_{\mathcal{N}}$. This uncertainty estimate will serve as a weight for the fit ensuring that automatically more weight is given to the larger model spaces for the determination of the parameters. It is not the aim to assign a realistic absolute uncertainty to each individual $E_{\mathcal{N}}$, but only to determine an estimate of the relative uncertainties of the different $E_{\mathcal{N}}$. We therefore assigned $\Delta E_{\mathcal{N}} = |E_{\mathcal{N}} - E_{\mathcal{N}+2}|$ for the uncertainty. For the largest model space \mathcal{N}_{\max} considered, we used the estimate of the previous model space. Therefore, the two largest model spaces contribute to the fit with equal weight. The errorbars obtained in this way are also shown in Fig. 6 together with the result of the fit. Our final binding energy is then given by E_{∞} . In order to obtain a conservative estimate of the uncertainty of this result, we assign $\Delta E_{\infty} = |E_{\infty} - E_{\mathcal{N}_{\max}}|$. E_{∞} and ΔE_{∞} are shown in the figures as red line and the surrounding shaded area.

Table 6 Ground state and excitation energies of ${}^3\text{H}$, ${}^4\text{He}$, ${}^6\text{He}$, ${}^6\text{Li}$ and ${}^7\text{Li}$ for different cutoff-parameters λ in comparison to the experimental values [37; 38]. * denotes ${}^6\text{He}$ excitation energies where the uncertainty estimate might not be reliable. See text for further explanations.

λ [fm $^{-1}$]	${}^3\text{H}$ [MeV]	${}^4\text{He}$ [MeV]	${}^6\text{He}$ [MeV]	${}^6\text{Li}$ [MeV]	${}^7\text{Li}$ [MeV]
1.0	-7.460	-24.271	-26.76(4)	-29.70(1)	-37.04(10)
			2.21(4) *	3.10(2)	0.133(2)
1.2	-7.929	-26.549	-28.76(10)	-31.77(8)	-39.68(28)
			2.42(7) *	3.08(1)	0.219(2)
1.5	-8.264	-28.173	-29.91(30)	-32.90(29)	-41.12(84)
			2.58(9) *	2.94(1)	0.335(9)
1.8	-8.332	-28.397(1)	-29.89(93)	-32.83(96)	-41.67(303)
			2.78(8) *	2.81(2)	0.420(27)
2.0	-8.314(4)	-28.189(3)	-29.80(191)	-32.80(204)	-41.50(505)
			2.72(7) *	2.76(3)	0.428(33)
2.2	-8.269(6)	-27.890(10)	-30.35(384)	-33.68(434)	-43.02(937)
			2.65(6) *	2.68(7)	0.421(39)
2.5	-8.184(11)	-27.378(23)	-34.26(1026)	-38.68(1192)	-51.72(2302)
			2.53(4) *	2.53(10)	0.443(60)
exp.	-8.482	-28.296	-29.271(54)	-31.994	-39.245(7)
			1.797(25)	2.186(2)	0.478(3)

Similar calculations have been performed for seven values of λ between 1.0 fm^{-1} and 2.5 fm^{-1} . The results for ${}^3\text{H}$ and all other nuclei considered in this work are summarized in Table 6. The energies for ${}^3\text{H}$ have been obtained with very high accuracy since we were able to obtain the cfp for very large model spaces for this system. We also note that the results for ${}^3\text{H}$ agree well with the results obtained by solving Faddeev equations [41].

5.2 ${}^4\text{He}$

The 3N system is an interesting test case since the convergence is quite slow because the nucleus is not very compact. So contributions from large \mathcal{N} can be tested. But since the cfp already separate the NN-subsystem, they do not test our transition coefficients to $2\text{N}-(A-2)\text{N}$ -states. Therefore, we consider as a second test nucleus ${}^4\text{He}$. Here, for the first time, the transition matrix elements enter. We expect however much faster convergence with respect to \mathcal{N} since the nucleus is more compact. At the same time, solutions of Yakubovsky equations [41] are available so that the results and the extrapolation procedure can be checked.

Fig. 7 shows the ω -dependence again for $\lambda = 1.5 \text{ fm}^{-1}$ and $\lambda = 2.5 \text{ fm}^{-1}$. It can be seen that, indeed, smaller \mathcal{N} are sufficient to get converged results. Again Eq. (33) gives a very good description of the ω -dependence of the results around the optimal values. In Fig. 8 the resulting \mathcal{N} -dependence of the energies is shown. Since the values of \mathcal{N} are now much smaller and since convergence is fast, our prescription to estimate the uncertainties leads to much stronger differences of the error estimates for different \mathcal{N} . This implies that the fit to Eq. (34) is dominated by the three largest model spaces. We observe that, also for this case, the binding energies can be extracted with high accuracy. We confirmed

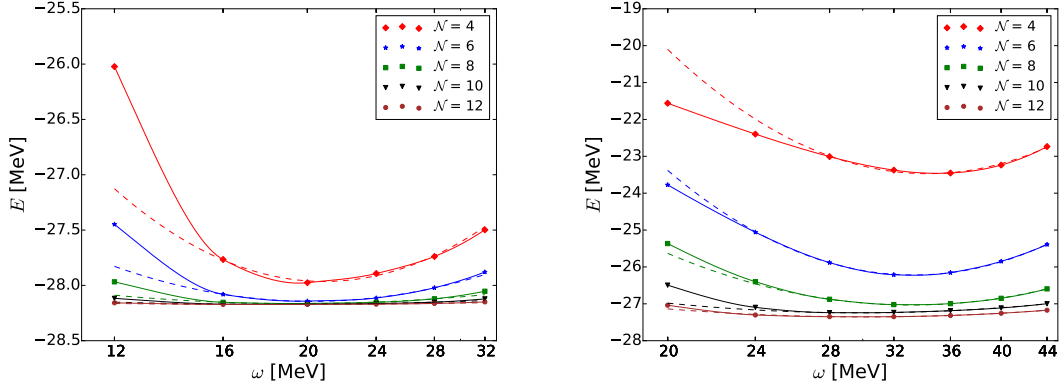


Fig. 7 ω -dependence of the ${}^4\text{He}$ binding energy for $\lambda = 1.5 \text{ fm}^{-1}$ (left) and $\lambda = 2.5 \text{ fm}^{-1}$ (right). Results for different model space sizes can be distinguished by the different markers and colors. The solid lines are added to guide the eye, the dashed lines are obtained using Eq. (33).

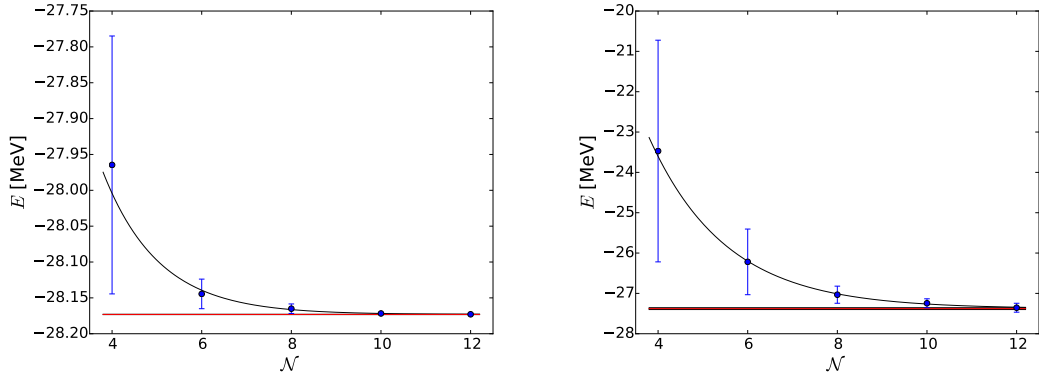


Fig. 8 \mathcal{N} -dependence of the ${}^4\text{He}$ binding energy for $\lambda = 1.5 \text{ fm}^{-1}$ (left) and $\lambda = 2.5 \text{ fm}^{-1}$ (right). The black line is obtained using Eq. (34). The result of the exponential extrapolation is indicated by the red line. The shaded area indicates the estimated uncertainty of the final result which is given by the difference of the result for the largest model space and the exponential extrapolation.

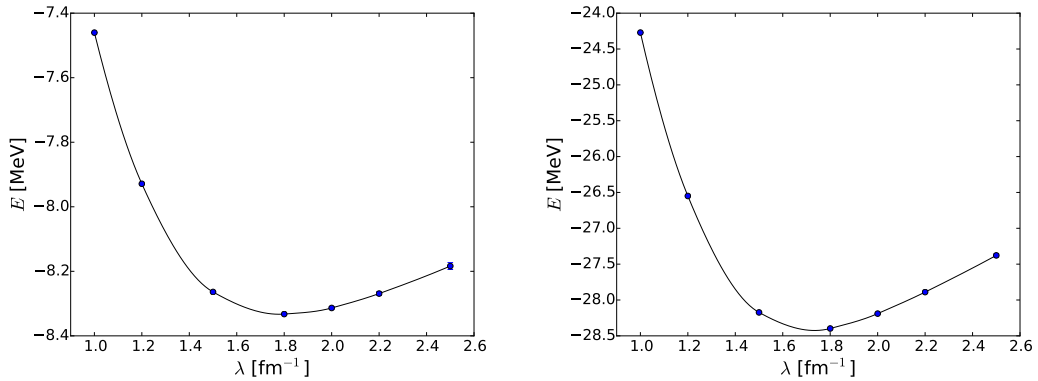


Fig. 9 λ -dependence of the ${}^3\text{H}$ (left) and the ${}^4\text{He}$ (right) binding energies. Errorbars indicating the uncertainties of the energies are too small to be seen.

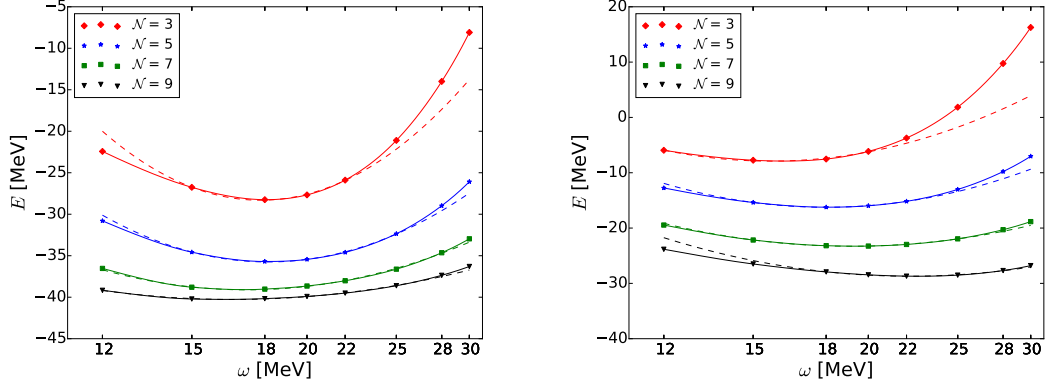


Fig. 10 ω -dependence of the ground state energy of ${}^7\text{Li}$ for $\lambda = 1.5 \text{ fm}^{-1}$ (left) and $\lambda = 2.5 \text{ fm}^{-1}$ (right). For lines and markers see Fig. 7.

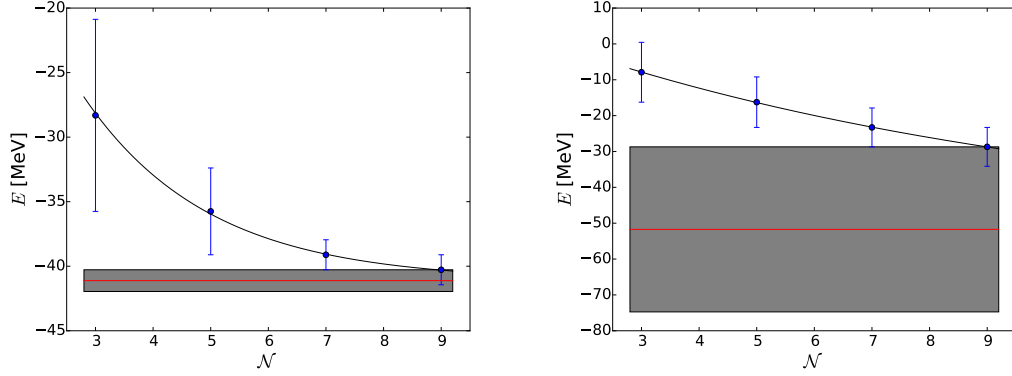


Fig. 11 \mathcal{N} -dependence of the ground state energy of ${}^7\text{Li}$ for $\lambda = 1.5 \text{ fm}^{-1}$ (left) and $\lambda = 2.5 \text{ fm}^{-1}$ (right). For lines and markers see Fig. 8.

that the extracted energies agrees with our solutions of Yakubovsky equations. Our results for ${}^4\text{He}$ are also summarized in Table 6.

Finally, we compare the λ -dependence of ${}^3\text{H}$ and ${}^4\text{He}$. It is well known that the two binding energies are strongly correlated and therefore it is not too surprising that the results follow the same trend. We just note that around $\lambda = 1.8 \text{ fm}^{-1}$, in the minimum, ${}^4\text{He}$ reaches the experimental value for its binding energy of -28.3 MeV . For ${}^3\text{H}$, the binding energy is also minimal for this value but does not reach the experimental value of -8.482 MeV .

5.3 ${}^7\text{Li}$

We now turn to the more difficult p -shell nuclei. Here, ${}^7\text{Li}$ is an interesting test case because the first excited state is really bound experimentally. So far, we have generated cfp up to $\mathcal{N} = 9$ for this system (see Appendix B). Our results for the ω and \mathcal{N} -dependence for this range of \mathcal{N} for the $J^\pi = \frac{3}{2}^-$ are summarized in Fig. 10 and 11. Again we show results for our two standard SRG cutoffs $\lambda = 1.5 \text{ fm}^{-1}$ and 2.5 fm^{-1} . For both cases, the ω -dependence can be described well by Eq. (33). But it is obvious that the model spaces used are not sufficient to obtain converged results for $\lambda = 2.5 \text{ fm}^{-1}$. Although the lines for different \mathcal{N} are getting closer, we observe that the optimal ω shifts to larger values with increasing \mathcal{N} . This implies that we do not find smaller steps for the extracted $E_{\mathcal{N}}$ when going to larger spaces as can be seen on the right of Fig. 11. The exponential extrapolation and the extracted

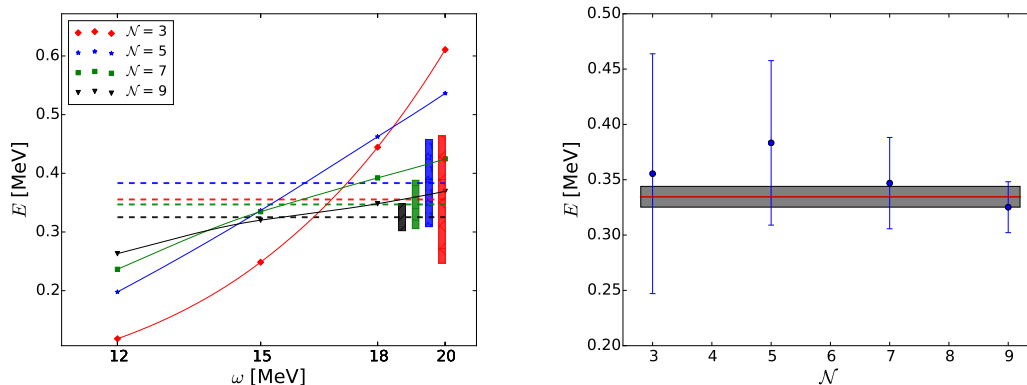


Fig. 12 Left hand side: ω -dependence of the excitation energy of ${}^7\text{Li}$ for $\lambda = 1.5 \text{ fm}^{-1}$. Markers indicate results for the excitation energy for different \mathcal{N} depending on ω . The lines connect results for the same \mathcal{N} to guide the eye. The extracted excitation energy and its uncertainty are given by the dashed lines and the box on the right of the graph. Right hand side: Extracted \mathcal{N} -dependence of the same excitation energy. The full result and its uncertainty are shown by the red solid line and the shaded box surrounding it.

uncertainty, which is also shown in the figure, clearly reflects that the model space size is too small to get converged results for this cutoff. This is not too worrisome since it is well known that once induced SRG 3N interactions are taken into account the λ -dependence becomes mild enough that much smaller values of λ are possible to get physically meaningful results [39]. For $\lambda = 1.5 \text{ fm}^{-1}$, we find the usual behavior as for the s -shell nuclei. The extracted $E_{\mathcal{N}}$ clearly show a pattern of convergence that allows for a meaningful extraction of the binding energy as shown on the left of Fig. 11.

Of course, similar calculations are possible for the excited state of ${}^7\text{Li}$. Such calculations show that the ground states and excited state binding energies are strongly correlated for NCSM calculations and that it is much more efficient to look directly at the excitation energies. For the first excited $J^\pi = \frac{1}{2}^-$ state of ${}^7\text{Li}$, we have calculated the excitation energy depending on the HO frequency and the model space size. For the example of $\lambda = 1.5 \text{ fm}^{-1}$, we show the results for the ω -dependence on the left hand side of Fig. 12. The excitation energies are used in a range that includes the two ω values right and left from the optimal ω values of the ground and excited state. It is reassuring that the ω -dependence flattens out when going to larger model spaces. In order to extract the excitation energy for a given \mathcal{N} , we calculated the average of the results of these ω . The uncertainty was then estimate by the standard deviation of the results from this average. Of course, since the ω range is chosen in an ad-hoc way, these uncertainties cannot be understood as absolute uncertainties. Still they indicate the errors for each \mathcal{N} relative to the others. In the second step, we therefore build a weighted average of the excitation energies for all \mathcal{N} where the weight is given by errors extracted from the ω -dependence. The results are shown on the right hand side of Fig. 12. In this way, we were able to obtain quite accurate results for the excitation energies.

To conclude this subsection, we finally show the λ -dependence for the binding energy of the ${}^7\text{Li}$ ground state and the excitation energy for the first excited state in Fig. 13. The uncertainties for both quantities are also shown. As discussed above, the model spaces used here are large enough for binding energies only for the lower λ below approximately 2 fm^{-1} . We find it however interesting that the excitation energies can be obtained fairly accurately even for larger λ . Again, we refer to Table 6 for the numerical values of the binding and excitation energies.

5.4 ${}^6\text{Li}$ and ${}^6\text{He}$

Finally, we present first results for $A = 6$ systems. We start with ${}^6\text{Li}$, for which we have prepared the cfp and transition coefficients for the $J^\pi = 1^+$ ground state and $J^\pi = 3^+$ excited state up to $\mathcal{N} = 10$. The ω -dependence is very similar to the one found for ${}^7\text{Li}$. Since we are now considering more HO excitations, the results are generally less dependent on the HO frequency than for $A = 7$. Therefore,

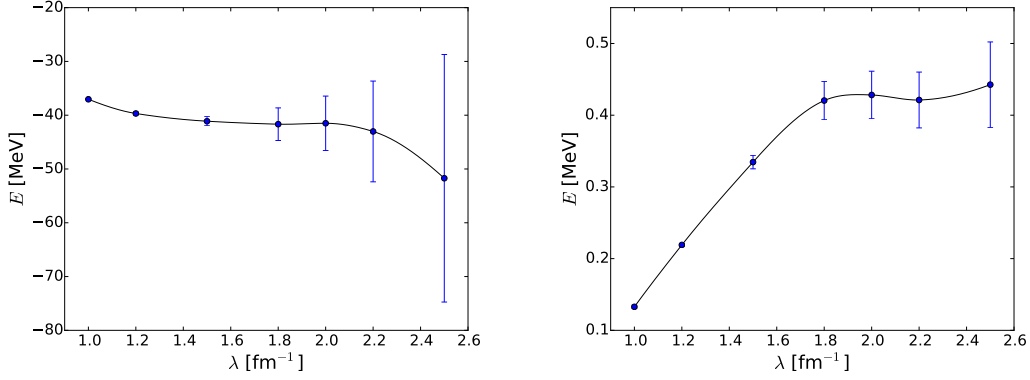


Fig. 13 λ -dependence of the ground state energy (left) and of the excitation energy (right) of ${}^7\text{Li}$. The uncertainties extracted as described in the text are given by the errorbars.

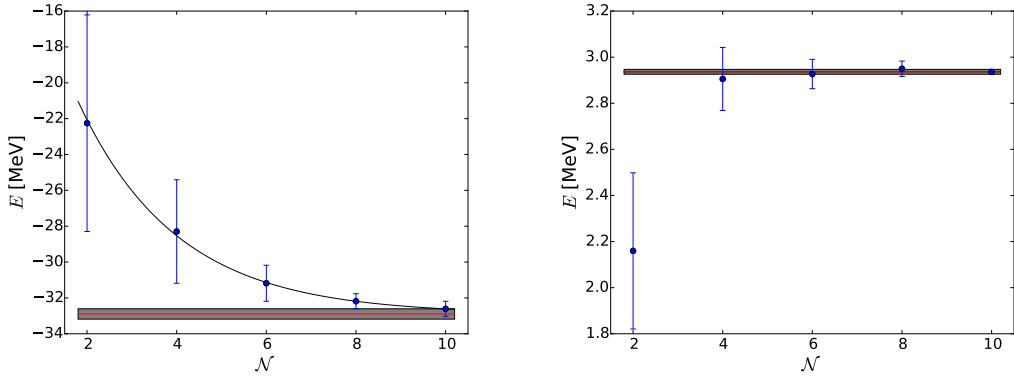


Fig. 14 \mathcal{N} -dependence of the ground state energy (left) and of the excitation energy (right) of ${}^6\text{Li}$ for $\lambda = 1.5 \text{ fm}^{-1}$. The full result and its uncertainty are shown by the red solid line and the shaded box surrounding it.

we directly present the \mathcal{N} -dependence for $\lambda = 1.5 \text{ fm}^{-1}$ in Fig. 14. As can be seen, the pattern of convergence is very regular for the binding energy and the excitation energy and the results are quite accurate. We note that the excited state is above the deuteron- ${}^4\text{He}$ threshold for many λ as it also is experimentally. Nevertheless, it is possible and regularly done to extract the excitation energy from NCSM calculations.

Fig. 15 (and the explicit values in Table 6) summarize our results for the binding energy and excitation energy for the full range of λ . It sticks out that the uncertainty estimates for $\lambda > 2 \text{ fm}^{-1}$ decrease again. This behavior seems unnatural and needs to be studied in larger model spaces in future.

For ${}^6\text{He}$, cfp also exist up to $\mathcal{N} = 10$ for the $J^\pi = 0^+$ ground state and the $J^\pi = 2^+$ excited state. We observe, that the pattern of convergence for the binding energy is again very similar to ${}^6\text{Li}$ and ${}^7\text{Li}$. Therefore, accurate results could be extracted as shown in Fig. 16. But, in this particular case, the results for the excitation energy of the $J^\pi = 2^+$ state were problematic. To exemplify this, we show in Fig. 17 the results for the ω -dependence of the excitation energies for $\lambda = 1.5 \text{ fm}^{-1}$. Here, even for this rather small λ , the ω -dependence is very small in all cases. But the changes when going to larger model spaces are large. The resulting \mathcal{N} -dependence is therefore very irregular. Since results for even lower cutoffs show a similar behavior, we refrain from showing the λ -dependence of the excitation energy. To provide benchmark results, we however included the numerical values of our automatized extraction procedure in Table 6. We stress however that the uncertainty estimates of the excitation energies for ${}^6\text{He}$ given in the table are probably not reliable.

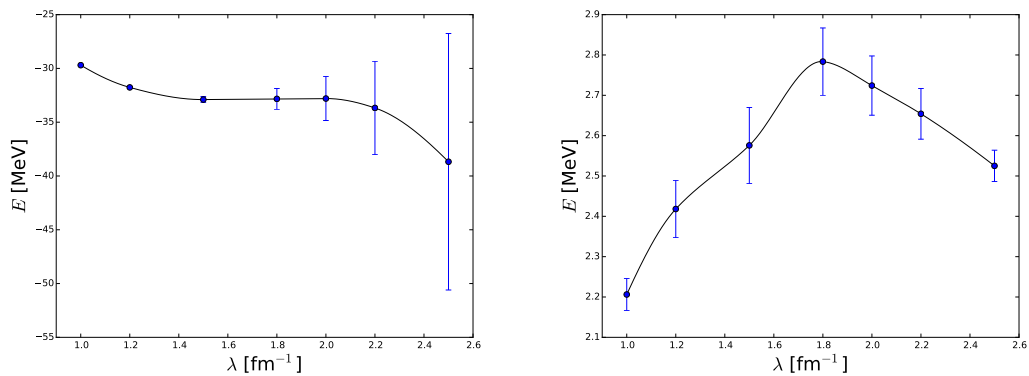


Fig. 15 λ -dependence of the ground state energy (left) and of the excitation energy (right) of ${}^6\text{Li}$.

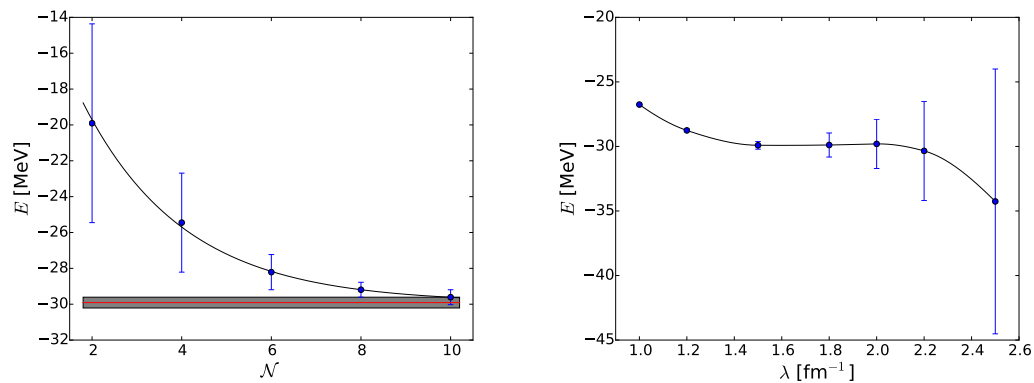


Fig. 16 \mathcal{N} -dependence for $\lambda = 1.5 \text{ fm}^{-1}$ (left) and λ -dependence (right) of the ground state energy of ${}^6\text{He}$.

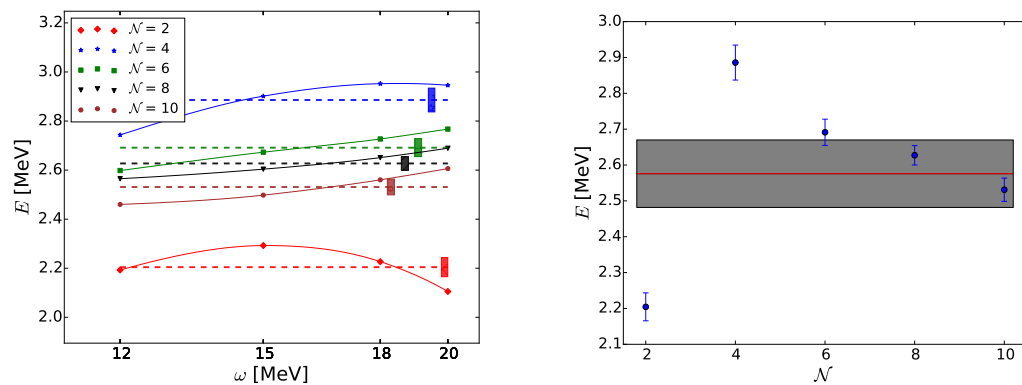


Fig. 17 Left hand side: ω -dependence of the excitation energy of ${}^6\text{He}$ for $\lambda = 1.5 \text{ fm}^{-1}$. Right hand side: Extracted \mathcal{N} -dependence of the same excitation energy. For an explanation of the notation see Fig. 12.

6 Conclusion and Outlook

In this work, we have described in detail a new implementation of cfp that allow one to perform NCSM calculations for light p -shell nuclei using relative coordinates. The use of relative coordinates separates off the CM motion and uses basis states with definite total angular momentum and isospin. Thereby, the dimension of the basis is considerably reduced. For the application of two-nucleon operators (e.g. NN forces), we introduced transition matrix elements to states that separate a two-nucleon cluster from the nucleus. These states enable a quite simple application of NN operators to A -nucleon states.

Once the cfp and transition elements are known, calculations for light p -shell nuclei require only modest computational resources. Therefore, as a first application, we applied the new basis set to s -shell and the lightest p -shell nuclei. We used the new set of basis states to map out the HO-frequency dependence of the results for increasing model space sizes and devised an automatized scheme to extract binding and excitation energies together with uncertainty estimates of the final results. The extraction procedure was applied to the s -shell nuclei as well as ${}^6\text{He}$, ${}^6\text{Li}$ and ${}^7\text{Li}$ and resulted in consistent results for all binding energies and the excitation energies of ${}^6\text{Li}$ and ${}^7\text{Li}$. For the excitation energy of ${}^6\text{He}$, the ω -dependence for the small model spaces turned out to be irregularly small and, therefore, the uncertainty estimates need to be checked using larger model spaces in future.

All these calculations were done with SRG evolved NN interactions for λ between 1.0 fm^{-1} and 2.5 fm^{-1} . We showed that within the model space, for which we have generated cfp so far, converged results could be obtained for $\lambda < 2.0 \text{ fm}^{-1}$. Recent NCSM calculations within the m -scheme have already shown that one obtains λ -insensitive results within this range of SRG parameters [39] once 3NFs have been included.

In order to be able to apply 3NFs, one more set of transition coefficients needs to be calculated. We also formulated the pertinent equations for these transitions. They have already been implemented and basic properties, like orthogonality, have been checked. Now they have to be accompanied by corresponding 3NF matrix elements. Work in this direction is in progress. In a very similar manner, such transitions can be extended to 4N and higher body operators. This is especially interesting since it is not clear at this point, whether 4NFs can give sizable contributions to p -shell binding energies. While the λ -dependence of the ${}^4\text{He}$ binding energy including induced 3NFs does not indicate significant contributions of 4N interactions [42], a direct calculation of the leading chiral 4NF revealed that a small net contribution is obtained because two sizable terms tend to cancel each other [21]. It needs to be clarified whether this cancelation is as effective in other systems. For this, the Jacobi NCSM will be an ideally suited tool since full use can be made of angular momentum and isospin conservation of the 4NF.

One important aspect of this work is to make the cfp and transition coefficients available. The corresponding data files have been generated using the HDF5 format and are platform independent. We hope that, in this way, nuclear structure calculations become simpler for other groups and can be applied to a wider range of problems. With the test calculations shown here, the cfp and NN transition coefficients are ready to be made accessible. The 3N transition coefficients will be made available, too, once they have been tested in similar calculations involving 3NFs.

Acknowledgements This work is supported in part by DFG and NSFC through funds provided to the Sino-German CRC 110 ‘‘Symmetries and the Emergence of Structure in QCD’’ (NSFC Grant No. 11261130311). The numerical calculations have been performed on JUQUEEN, JUROPA and JURECA of the JSC, Jülich, Germany.

A HO wave functions R_{nl} in coordinate and momentum space

cfp and transition coefficients rely on the Talmi-Moshinsky brackets of Ref. [28]. In this appendix, we shortly summarize the conventions for the HO wave functions related the conventions used in this work. We define the dimensionless HO wave functions

$$\hat{R}_{nl}(\rho) = (-1)^n \left[\frac{2n!}{\Gamma(n+l+\frac{3}{2})} \right]^{\frac{1}{2}} \exp\left(-\frac{\rho^2}{2}\right) \rho^l L_n^{(l+\frac{1}{2})}(\rho^2) . \quad (35)$$

The configuration space R_{nl} are just given by a simple rescaling involving the HO length b :

$$R_{nl}(r) = b^{-\frac{3}{2}} \hat{R}_{nl}\left(\frac{r}{b}\right) . \quad (36)$$

The momentum space wave function is then obtained by a Fourier transformation

$$R_{nl}(p) = \sqrt{\frac{2}{\pi}} i^l \int dr r^2 j_l(pr) R_{nl}(r) \quad (37)$$

that leads to

$$R_{nl}(p) = (-1)^n i^l b^{\frac{3}{2}} \hat{R}_{nl}(bp) \quad (38)$$

Note that matrix elements that are parity conserving will only acquire a real phase due to the i^l factor.

B Existing cfp and transition coefficients

In this appendix, we summarize the cfp and transition coefficients that have already been generated. More sets of coefficients are currently generated.

The following table shows the available sets of cfp for the $A = 3$ to $A = 7$ system. Ranges of J , T and $Ntot$ values of calculated blocks are given. The label complete indicates that sets for all J and T possible for the given $Ntot$ are available.

	J	T	\mathcal{N}	
$A = 3$	$\frac{1}{2}, \dots, \frac{51}{2}$	$\frac{1}{2}, \frac{3}{2}$	$0, \dots, 24$	(complete)
$A = 4$	$0, \dots, 14$	$0, \dots, 2$	$0, \dots, 12$	(complete)
$A = 5$	$\frac{1}{2}, \dots, \frac{25}{2}$	$\frac{1}{2}, \dots, \frac{5}{2}$	$1, \dots, 10$	(complete)
$A = 6$	$0, \dots, 13$	$0, \dots, 3$	$2, \dots, 10$	(complete)
$A = 7$	$\frac{1}{2}, \dots, \frac{25}{2}$	$\frac{1}{2}, \dots, \frac{7}{2}$	$3, \dots, 9$	(complete)

The next table summarizes the same for $2N+(A-2)N$ transition coefficients. At this point, the $A = 4$ system is complete for $\mathcal{N} \leq 10$. In the other cases, isospins and angular momenta correspond to the states of selected nuclei. Again, more sets of matrix elements are generated currently.

	J	T	\mathcal{N}	
$A = 4$	$0, \dots, 12$	$0, \dots, 2$	$0, \dots, 10$	(complete)
${}^4\text{He}$	0	0	11,12	
${}^6\text{Li}$	1, 2, 3	0	2, \dots, 10	
${}^6\text{He}$	0, 2	1	2, \dots, 10	
${}^7\text{Li}$	$\frac{1}{2}, \frac{3}{2}$	$\frac{1}{2}$	3, \dots, 9	

References

1. W. Glöckle, H. Witała, D. Hüber, H. Kamada, and J. Golak, Phys. Rep. **274**, 107 (1996).
2. A. Nogga, H. Kamada, and W. Glöckle, Phys. Rev. Lett. **85**, 944 (2000).
3. R. Lazauskas, Phys. Rev. C **91**, 041001 (2015).
4. A. Deltuva and A. C. Fonseca, Phys. Rev. C **76**, 021001 (2007).
5. M. Viviani, A. Kievsky, and S. Rosati, Phys. Rev. C **71**, 024006 (2005).
6. N. Barnea, W. Leidemann, and G. Orlandini, Phys. Rev. C **81**, 064001 (2010).
7. M. A. Caprio, P. Maris, and J. P. Vary, Phys. Rev. C **86**, 034312 (2012).
8. B. R. Barrett, P. Navrátil, and J. P. Vary, Prog. Part. Nucl. Phys. **69**, 131 (2013).
9. R. Roth and P. Navrátil, Phys. Rev. Lett. **99**, 092501 (2007).
10. C. Forssén, E. Caurier, and P. Navrátil, Phys. Rev. C **79**, 021303 (2009).

11. I. Stetcu, B. R. Barrett, P. Navrátil, and J. P. Vary, *Phys. Rev. C* **71**, 044325 (2005).
12. U.-G. Meißner (2015), [arXiv:1509.08290\[nucl-th\]](https://arxiv.org/abs/1509.08290).
13. A. Nogga, P. Navrátil, B. R. Barrett, and J. P. Vary, *Phys. Rev. C* **73**, 064002 (2006).
14. P. Navrátil, V. G. Gueorguiev, J. P. Vary, W. E. Ormand, and A. Nogga, *Phys. Rev. Lett.* **99**, 042501 (2007).
15. S. Binder, A. Calci, E. Epelbaum, R. J. Furnstahl, J. Golak, K. Hebeler, H. Kamada, H. Krebs, J. Langhammer, S. Liebig, et al., pp. 1–5 (2015).
16. P. Navrátil, G. P. Kamuntavičius, and B. R. Barrett, *Phys. Rev. C* **61**, 044001 (2000).
17. E. Epelbaum, H.-W. Hammer, and U.-G. Meißner, *Rev. Mod. Phys.* **81**, 1773 (2009).
18. R. Machleidt and D. R. Entem, *Phys. Rep.* **503**, 1 (2011).
19. E. Epelbaum, *Phys. Lett. B* **639**, 456 (2006).
20. E. Epelbaum, *Eur. Phys. J. A* **34**, 197 (2007).
21. A. Nogga, E. Epelbaum, J. Golak, H. Kamada, H. Witała, D. Rzepdzik, R. Skibinski, and W. Glöckle, in *19th International IUPAP Conference on Few-Body Problems in Physics* (2010), p. 05006.
22. P. Navrátil and W. E. Ormand, *Phys. Rev. Lett.* **88**, 152502 (2002).
23. S. K. Bogner, T. T. S. Kuo, and A. Schwenk, *Phys. Rep.* **386**, 1 (2003).
24. S. K. Bogner, R. J. Furnstahl, and R. J. Perry, *Phys. Rev. C* **75**, 061001 (2007).
25. E. D. Jurgenson, P. Navrátil, and R. J. Furnstahl, *Phys. Rev. Lett.* **103**, 082501 (2009).
26. I. Talmi, *Helvetica Physica Acta* **25**, 185 (1952).
27. M. Moshinsky, *Nucl. Phys.* **13**, 104 (1959).
28. G. P. Kamuntavičius, R. K. Kalinauskas, B. R. Barrett, S. Mickevičius, and D. Germanas, *Nucl. Phys. A* **695**, 191 (2001).
29. G. Racah, *Phys. Rev.* **63**, 367 (1943).
30. L. S. Blackford, J. Choi, A. Cleary, E. D’Azevedo, J. Demmel, I. Dhillon, J. Dongarra, S. Hammarling, G. Henry, A. Petitet, et al., *ScaLAPACK Users’ Guide* (SIAM, 1997).
31. T. Auckenthaler, H. J. Bungartz, T. Huckle, L. Krämer, B. Lang, and P. Willems, *Journal of Computational Science* **2**, 272 (2011).
32. The HDF Group (1997).
33. S. Liebig, Ph.D. thesis, Bonn University (2013).
34. D. R. Entem and R. Machleidt, *Phys. Rev. C* **68**, 041001 (2003).
35. G. P. Kamuntavičius, P. Navrátil, B. R. Barrett, G. Sapragnaite, and R. K. Kalinauskas, *Phys. Rev. C* **60**, 044304 (1999).
36. R. B. Wiringa, V. G. J. Stoks, and R. Schiavilla, *Phys. Rev. C* **51**, 38 (1995).
37. G. Audi, M. Wang, A. H. Wapstra, F. G. Kondev, M. MacCormick, X. Xu, and B. Pfeiffer, *Chinese Phys. C* **36**, 1287 (2012).
38. D. R. Tilley and others, *Nucl. Phys. A* **708**, 3 (2002).
39. E. D. Jurgenson, P. Maris, R. J. Furnstahl, P. Navrátil, W. E. Ormand, and J. P. Vary, *Phys. Rev. C* **87**, 054312 (2013).
40. R. J. Furnstahl, G. Hagen, T. Papenbrock, and K. A. Wendt, *J. Phys. G* **42**, 034032 (2015).
41. A. Nogga, H. Kamada, W. Glöckle, and B. R. Barrett, *Phys. Rev. C* **65**, 054003 (2002).
42. E. D. Jurgenson, P. Navrátil, and R. J. Furnstahl, *Phys. Rev. C* **83**, 034301 (2011).